Clinical Cancer Research

Quantitative Ultrasound Spectroscopy for Differentiation of Hepatocellular Carcinoma from At-Risk and Normal Liver Parenchyma

Isabelle Durot[1,2], Rosa M.S. Sigrist[1,2], Nishita Kothary[1], Jarrett Rosenberg[1], Jürgen K. Willmann[1,2,†], and Ahmed El Kaffas[1,2]

Abstract

Purpose: Quantitative ultrasound approaches can capture tissue morphologic properties to augment clinical diagnostics. This study aims to clinically assess whether quantitative ultrasound spectroscopy (QUS) parameters measured in hepatocellular carcinoma (HCC) tissues can be differentiated from those measured in at-risk or healthy liver parenchyma.

Experimental Design: This prospective Health Insurance Portability and Accountability Act (HIPAA)–compliant study was approved by the Institutional Review Board. Fifteen patients with HCC, 15 non-HCC patients with chronic liver disease, and 15 healthy volunteers were included (31.1% women; 68.9% men). Ultrasound radiofrequency data were acquired in each patient in both liver lobes at two focal depths (3/9 cm). Region of interests (ROIs) were drawn on HCC and liver parenchyma. The average normalized power spectrum for each ROI was extracted, and a linear regression was fit within the −6 dB bandwidth, from which the midband fit (MBF), spectral intercept (SI), and spectral slope (SS) were extracted. Differences in QUS parameters between the ROIs were tested by a mixed-effects regression.

Results: There was a significant intraindividual difference in MBF, SS, and SI between HCC and adjacent liver parenchyma ($P < 0.001$), and a significant interindividual difference between HCC and at-risk and healthy non-HCC parenchyma ($P < 0.001$). In patients with HCC, cirrhosis ($n = 13$) did not significantly change any of the three parameters ($P > 0.8$) in differentiating HCC from non-HCC parenchyma. MBF ($P = 0.12$), SI ($P = 0.33$), and SS ($P = 0.57$) were not significantly different in non-HCC tissue among the groups.

Conclusions: The QUS parameters are significantly different in HCC versus non-HCC liver parenchyma, independent of underlying cirrhosis. This could be leveraged for improved HCC detection with ultrasound in the future.

Introduction

Hepatocellular carcinoma (HCC) is the sixth most common cause of cancer and the second most common cause of cancer-related deaths worldwide (1, 2). Most cases of HCC develop in patients with chronic liver disease on a background of liver cirrhosis (3, 4). HCC is a highly aggressive tumor with a poor prognosis when diagnosed at late stage, also leading to a considerable economic burden in particular in developing countries (5, 6). Thus, early detection of HCC is of paramount importance to improve treatment options and reduce mortality. In the United States, contrast-enhanced MRI is currently the most accurate modality to diagnose HCC (7), although beyond reach for most of the population worldwide with a high incidence of chronic liver disease and 85% of the global tumor burden (8) occurring in developing countries. The European and Asian guidelines on managing HCC recommend a biannual B-mode ultrasound as first-line imaging exam for HCC screening in high-risk patients (9). However, conventional ultrasound as screening tool has limited sensitivity and specificity, in particular in patients with liver cirrhosis, with sensitivities as low as 60% for detecting HCC in cirrhosis (10, 11). Therefore, further improvement of the diagnostic accuracy of readily accessible and inexpensive ultrasound for detecting HCC is critically needed.

In recent years, several quantitative ultrasound techniques have gained significant interest as means to improve the detection and characterization of tissue features, and augment clinical diagnostics (12). One of these techniques is quantitative ultrasound spectroscopy (QUS), which was first promulgated by Lizzi and colleagues in the early 1980s (13). QUS can provide quantitative information related to tissue characteristics using standard ultrasound systems (12), and allows differentiation of tissue microstructures by analyzing the radiofrequency (RF) signals backscattered from biological tissues (14). It is independent of instrument settings through a signal normalization process that uses a reference phantom with known backscatter and attenuation coefficients (12, 15–17). Because QUS uses the raw RF signal used to construct the conventional B-mode images, the technique could be included in routine ultrasound screening protocols of the liver, and may improve HCC detection in this setting due to additional quantitative information. The already widespread availability of B-mode ultrasound for hepatic imaging is further

[1]Department of Radiology, School of Medicine, Stanford University, Stanford, California. [2]Translational Molecular Imaging Lab, School of Medicine, Stanford University, Stanford, California.

Note: Supplementary data for this article are available at Clinical Cancer Research Online (http://clincancerres.aacrjournals.org/).

[†]Deceased.

Corresponding Author: Ahmed El Kaffas, Stanford University School of Medicine, 300 Pasteur Drive, Stanford, CA 94306. Phone: 650-353-6495; Fax: 650-723-1909; E-mail: elkaffas@stanford.edu

Clin Cancer Res 2019;25:6683–91

doi: 10.1158/1078-0432.CCR-19-1030

Translational Relevance

Quantitative ultrasound spectroscopy (QUS) of the liver using the midband fit, spectral intercept, and spectral slope parameters allows differentiation between hepatocellular carcinoma (HCC) and non-HCC liver parenchyma, at-risk liver, and normal liver parenchyma. This is independent of the status of the non-HCC liver parenchyma (cirrhotic vs. non-cirrhotic; at risk or normal) and the fasting state in healthy volunteers. QUS could be included in routine ultrasound screening protocols of the liver for early detection of HCC in at-risk patients without extending the acquisition time, because QUS methods rely on the acquisition of conventional B-mode ultrasound images and accompanying radiofrequency data. In particular, in patients with cirrhosis where standard B-mode ultrasound screening may be limited, QUS may add quantitative information and clinical value. Early detection of HCC with a widely available and inexpensive method improves the management and survival of liver cancer, especially in developing high-incidence countries.

supported by known advantages such as relatively low cost, portability, and the lack of ionizing radiation. Nonetheless, although RF data are increasingly available on commercial systems, it remains a challenge to get access to these data from major commercial companies.

Besides a small pilot study in 1985 that first evaluated QUS in a small number of patients with alcoholic liver disease and six different focal liver lesions (18), there is no published literature on QUS assessment of liver parenchyma versus HCC which is needed to further clinically develop QUS for HCC detection.

Therefore, the purpose of this study was to clinically assess QUS parameters in HCC compared with at-risk and healthy liver parenchyma.

Materials and Methods

This HIPAA-compliant prospective study was approved by the Institutional Review Board of our institution, and written consent was obtained from all patients.

Patient population

From May 2016 to June 2017, 30 consecutive patients and 15 healthy subjects were enrolled in this study. From the enrollment start date, patients were subdivided into three groups of 15 patients (Fig. 1 and Table 1); 31 of 45 (68.9%) were men (mean age, 52.4 years; range, 29–84 years), and 14 of 45 (31.1%) patients were women (mean age, 45.8 years; range, 24–66 years). Difference in age and gender are due to consecutive enrollment.

The first group (henceforth called patients with HCC) included 15 patients (11 men; mean age, 65.5 years; range, 49–84 years; four women; mean age, 65.8 years; range, 62–70 years) with HCC and chronic liver disease (11 chronic hepatitis C; one polycythemia vera; one hemochromatosis; one nonalcoholic steatohepatitis; one cryptogenic cirrhosis). HCC was confirmed by multiphase contrast-enhanced CT ($n = 6$) or MRI (gadolinium-based contrast agents ; $n = 9$) using the Organ Procurement Transplantation Network classification system. Both of these tests are considered the standard of care at our institute to diagnose HCC (19). Patients were scheduled for transarterial chemoembolization after QUS imaging. Thirteen of 15 patients (86.7%) had liver cirrhosis, diagnosed with ultrasound or MR elastography. The mean diameter of HCC was 3.2 cm (range, 1.4–7.2 cm); and 12 of 15 (80.0%) patients had one HCC nodule, one of 15 (6.7%) had two HCC nodules, and two of 15 (13.3%) had three HCC nodules. Seven of 15 HCCs (46.7%) were located in the left liver lobe, and eight of 15 (53.3%) in the right lobe. Patients with prior HCC treatment, taking investigational agents, unable to sign written consent or with diagnosis other than HCC were excluded; two patients were excluded from the study due to exclusion criteria.

The second group (henceforth called at-risk patients) included 15 patients (10 men; mean age, 57.6 years; range, 33–79 years; five women; mean age, 41.4 years; range, 24–58 years) with chronic liver disease but without HCC (seven chronic hepatitis B; seven chronic hepatitis C; one cryptogenic cirrhosis). These patients were part of a biannual ultrasound screening program at our institution, and on the same day of the QUS acquisition, a routine clinical hepatoma survey ultrasound exam of the liver was performed with no evidence for HCC.

The third group (henceforth called healthy volunteers) included 15 volunteers that underwent a medical check-up within 6 months of the ultrasound exam without any signs of acute or chronic liver disease. In this group, 10 patients were men (mean age, 32.9 years; range, 28–38 years) and five patients were women (mean age, 33.2 years; range, 30–37 years).

System and acquisition parameters

In all patients, liver imaging was performed using a clinical ultrasound scanner (Ultrasonix Tablet; Analogic Corporation), coupled to a broadband 3- to 7-MHz transducer (Ultrasonix; C7–3/50; curved array). All patients were asked to fast for a minimum 8 hours prior to the ultrasound exam. All acquisitions were performed by one of two board-certified radiologists with 3 and 4 years, respectively, of experience in liver ultrasound imaging. During acquisition, patients were placed in supine position, and data were acquired in inspiration. Imaging protocol consisted of a total of 32 ultrasound data acquisition in the non-HCC liver tissue to evaluate different settings, and surveying both liver lobes in both a transversal and sagittal plane. For each of the acquisition, both regular B-mode images and RF data were acquired using the 3.3- and 5-MHz frequency settings, and at two focal depths (3 and 9 cm); the latter were chosen because all lesions were classified in the depth range of 0–6 cm or 6–12 cm, and the sonographer took steps to ensure that the lesion was as close as possible to the 3- or 9-cm focus zone. All other imaging parameters were kept consistent throughout all scans (gain, 55%; power, 0 W; imaging depth, 15 cm; TGC, centered; frame rate per second, 23; dynamic range, 68 dB). In all patients with confirmed HCC, the sonographer was able to identify the target lesion on B-mode ultrasound, and 16 additional acquisitions were made with the HCC in the imaging plane. Overall, scan sessions lasted 10 to 15 minutes.

Furthermore, to determine whether QUS parameters measured in the liver parenchyma are affected by the fasting state of patients, two QUS exams using the same imaging protocol (Table 2) were performed on the same day in all 15 healthy volunteers. The first scan was carried out after a fasting period of at least 8 hours; the second scan 30 minutes after a 400 to 500 calories meal to break the fast.

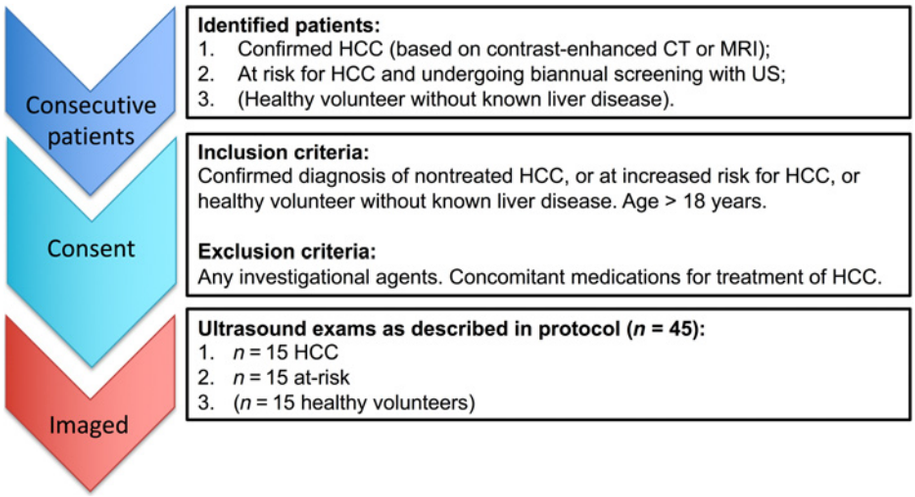

Figure 1.
Summary of patient enrollment protocol based on inclusion/exclusion criteria and consent.

All data were saved on a secure external hard drive for subsequent data analysis.

Quantification of ultrasound spectroscopy data

All QUS analysis was carried out using MATLAB (MathWorks) to compute the established QUS parameters midband fit (MBF), spectral slope (SS), and spectral intercept (SI), as summarized in Supplementary Fig. S1, and as previously described in (20). More specifically, analysis consisted of the following steps: (1) drawing regions of interest (ROI) on liver parenchyma (ROI diameter range, 3–5 cm, depending on image and focus depth) and/or HCC (ROI size similar to HCC size; HCC identification on B-mode image with help of MRI or CT) for each ultrasound setting in regions to be analyzed (Supplementary Fig. S1A); (2) discretization of ROI into as many windows as can fit into the ROI with each window overlapping its neighbors by 80%; each window was set at 4 x 4 mm for quantitative analysis (Supplementary Fig. S1A)—the windows allow to compute the QUS parameters at different spatial locations to obtain parametric maps; (3) for each window, a Fourier-transform (FFT) was then used to obtain the power spectrum (PS) in the liver image, as well as the reference PS (rPS) from a matching RF image (all parameters matching in both images, including depth, width, and focus) of a reference phantom (Supplementary Fig. S1B); (4) we then divide the PS by the rPS to obtain the normalized PS (NPS; Supplementary Fig. S1B)—the normalization process reduces the influence of system properties/transfer functions, beam-forming, artifacts, and instrument settings on spectroscopic analysis, rendering it a more quantitative technique than attempting to extract parameters on non-normalized data. Normalization can also minimize depth-related attenuation effects (21); (5) a linear-regression fit to the NPS was then used to obtain the QUS parameters (Supplementary Fig. S1C; refs. 13, 22, 23). In step 3, the PS was estimated by taking the square of the magnitude of the fast FFT of the Hamming-gated RF echo segment $e_s(t, x_i)$, as a function of time (t) and lateral position (x_i) for each scan line in each window within the ROI. An average power spectrum was obtained for each of the windows within each ROI. For step 4, all data were normalized to obtain the NPS using the established reference phantom method, using the rPS obtained from the RF echo segment $e_p(t, x_i)$ (obtained from a custom-made phantom by CIRS; ref. 16). The phantom used here has a speed of sound of 1,560 ± 10 m/s, an attenuation coefficient of 0.50 ± 0.05 dB/cm/MHz, and a backscatter coefficient at 3 MHz of 10^{-3} $(\text{str}^*\text{cm})^{-1}$. The phantom was scanned after acquisition of B-mode images in all patients to enable calibration. Hence, the power spectrum for each ROI can be obtained from Equation (1):

$$S(f) = \frac{\sum_{i=M}^{N} \left|\text{FFT}(\text{Hamming}(e_s(t, x_i))\right|^2}{\sum_{i=M}^{N} \left|\text{FFT}\left(\text{Hamming}(e_p(t, x_i)\right)\right|^2} \quad (1)$$

where $i = M, M+1, \ldots, N$ RF lines in the ROI window. For step 5, quantitative spectral parameters were derived from a linear-regression approximation (in logarithmic scale) within a –6 dB window to the NPS, centered at the transducer center frequency (determined from calibration pulse). The following parameters were obtained: the SS (slope of line-approximation), the 0-MHz SI (y axis intercept of line-approximation), the MBF (solution of line-approximation at the center frequency of –6 dB bandwidth). These parameters are related to the scatterer size (SI, SS), the acoustics scatterer concentration (MBF, SI), or differences in acoustic impedance between the scatterer and its surrounding medium (SI). More specifically, parameters were obtained using the following Equations (2 and 3), where f_c is the central frequency:

$$S(f) = \text{SS} \times f + \text{SI} \quad (2)$$

$$\text{MBF} = S(f_c) \quad (3)$$

Spectral parameters for each image plane were obtained through averaging in an ROI on spatial parametric maps of MBF, SS, and SI (Fig. 2).

Maps were generated using a sliding window analysis on a pixel-by-pixel basis within ROIs (encompassing the lesion, or corresponding parenchyma at same depth), where spectral parameters were computed within each window within the ROI (Supplementary Fig. S1A). Each window was normalized separately to a reference curve obtained from the exact same region of the corresponding phantom image (obtained with same parameters), with equivalent localization and dimensions. Figure 3 displays parametric images within large ROIs encompassing

Table 1. Summary of patient information in the three different patients groups ($n = 15$ each)

Number	Group	Age	Gender	Ethnic group	Liver disease	Fibrosis stage	Location HCC[a]	Diameter HCC (cm)
1	HCC	53	Male	Caucasian	HCV	F4	IVb	2.8
2	HCC	66	Female	Caucasian	HCV	F4	IVa	2.9
3	HCC	49	Male	Hispanic	HCV	F4	II/III	7.0
4	HCC	79	Male	Caucasian	Polycythemia vera	F0/F1	VIII	7.1
5	HCC	67	Male	Caucasian	NASH	F4	III	2.0
6	HCC	48	Male	Unknown	HCV	F4	VI	5.0
7	HCC	62	Female	Caucasian	HCV	F4	IVb	1.4
8	HCC	75	Male	Caucasian	HCV	F4	VII	3.0
9	HCC	63	Male	Asian	HCV	F4	VI/VII	2.2
10	HCC	56	Male	Caucasian	HCV	F4	VI	3.0
11	HCC	70	Female	Asian	HCV	F4	III	2.3
12	HCC	65	Female	Hispanic	Cryptogenic cirrhosis	F4	V	2.6
13	HCC	73	Male	Caucasian	HCV	F4	VIII	2.0
14	HCC	73	Male	Asian	HCV	F4	IVa	1.9
15	HCC	84	Male	Caucasian	Hemochromatosis	F0/F1	VI	2.6
16	At-risk	67	Male	Caucasian	HCV	F4		
17	At-risk	61	Male	Asian	HBV	F0/F1		
18	At-risk	66	Male	Asian	HBV	F2		
19	At-risk	79	Male	Caucasian	Cryptogenic cirrhosis	F4		
20	At-risk	59	Male	Hispanic	HCV	F4		
21	At-risk	58	Male	Asian	HBV	F0/F1		
22	At-risk	44	Male	Hispanic	HCV	F0/F1		
23	At-risk	46	Female	Hispanic	HCV	F4		
24	At-risk	45	Male	Asian	HBV	F0/F1		
25	At-risk	24	Female	Asian	HBV	F2		
26	At-risk	45	Female	Asian	HBV	F0/F1		
27	At-risk	64	Male	Caucasian	HCV	F0/F1		
28	At-risk	34	Female	Arabian	HCV	F0/F1		
29	At-risk	58	Female	Caucasian	HCV	F4		
30	At-risk	33	Male	Asian	HBV	F0/F1		
31	HV	34	Male	Asian	None	F0/F1		
32	HV	36	Male	Caucasian	None	F0/F1		
33	HV	36	Male	Caucasian	None	F0/F1		
34	HV	36	Female	Caucasian	None	F0/F1		
35	HV	38	Male	Arabian	None	F0/F1		
36	HV	28	Male	Asian	None	F0/F1		
37	HV	29	Male	Arabian	None	F0/F1		
38	HV	32	Male	Caucasian	None	F0/F1		
39	HV	37	Male	Caucasian	None	F0/F1		
40	HV	37	Female	Caucasian	None	F0/F1		
41	HV	29	Male	Asian	None	F0/F1		
42	HV	30	Male	Asian	None	F0/F1		
43	HV	32	Female	Arabian	None	F0/F1		
44	HV	31	Female	Caucasian	None	F0/F1		
45	HV	30	Female	Caucasian	None	F0/F1		

Abbreviations: HBV, hepatitis B; HCV, hepatitis C; HV, healthy volunteer; NASH, nonalcoholic steatohepatitis.
[a]Location of HCC refers to liver segments I–VIII.

visible liver tissue, which were produced using a sliding window with a time bandwidth product of approximately 10 (12). For each of these processed images, the dynamic range is set to –25 dB to 5 dB, which was optimized to enhance contrast in HCC tissue versus parenchyma tissue.

Statistical analysis

The effects of age, gender, liver lobe, frame number frequency, focal depth, and imaging plane (transverse vs. sagittal) in all groups on QUS parameters MBF, SI, and SS were tested by a mixed-effects multivariable-regression model

Table 2. Summary of mean values for MBF, SI, and SS

Group	MBF (dB)	SI (dB)	SS (dB/MHz)	Statistical significance
HCC				
Lesion	−3.6 (SD 2.9)	6.4 (SD 3.1)	−1.7 (SD 0.6)	
Parenchyma[a]	3.9 (SD 0.8)	19.3 (SD 3.3)	−2.6 (SD 0.8)	$P < 0.001$[b]
At-risk				
Parenchyma[a]	3.5 (SD 2.6)	19.7 (SD 3.6)	−2.8 (SD 0.5)	$P < 0.001$[b]
Healthy volunteers				
Parenchyma[a]: Preprandial	3.1 (SD 1.5)	19.1 (SD 3.3)	−2.6 (SD 0.5)	$P < 0.001$[b]
Parenchyma[a]: Postprandial	3.1 (SD 1.5)	19.0 (SD 3.3)	−2.7 (SD 0.5)	$P < 0.001$[b]

[a]Parenchyma refers to measurements obtained in non-HCC liver parenchyma.
[b]Statistical significance refers to the comparison of the values obtained in the HCC lesions (HCC group) with the non-HCC liver parenchyma (all groups).

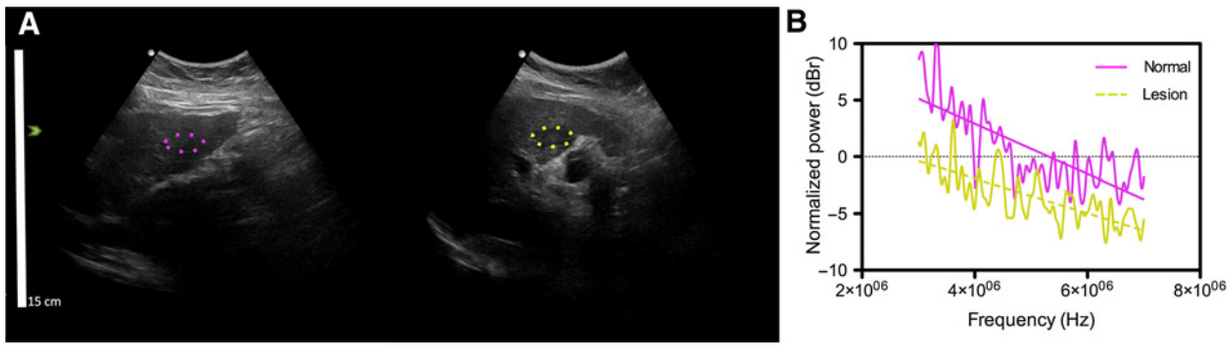

Figure 2.

A, Two separate images in same patient (65-year-old woman with cryptogenic liver cirrhosis and confirmed HCC in segment V). The left image is of liver parenchyma in the left liver lobe, whereas the right image is of a lesion (2.2 × 1.8 cm) confirmed with MRI. **B,** A graph showing the NPS of a single largest rectangular window fitting within the purple (normal tissue) or yellow (lesion) ROI. The NPS is used to compute QUS parameters MBF, SI, and SS using a linear-regression fit to the NPS (shown here as a line through the NPS).

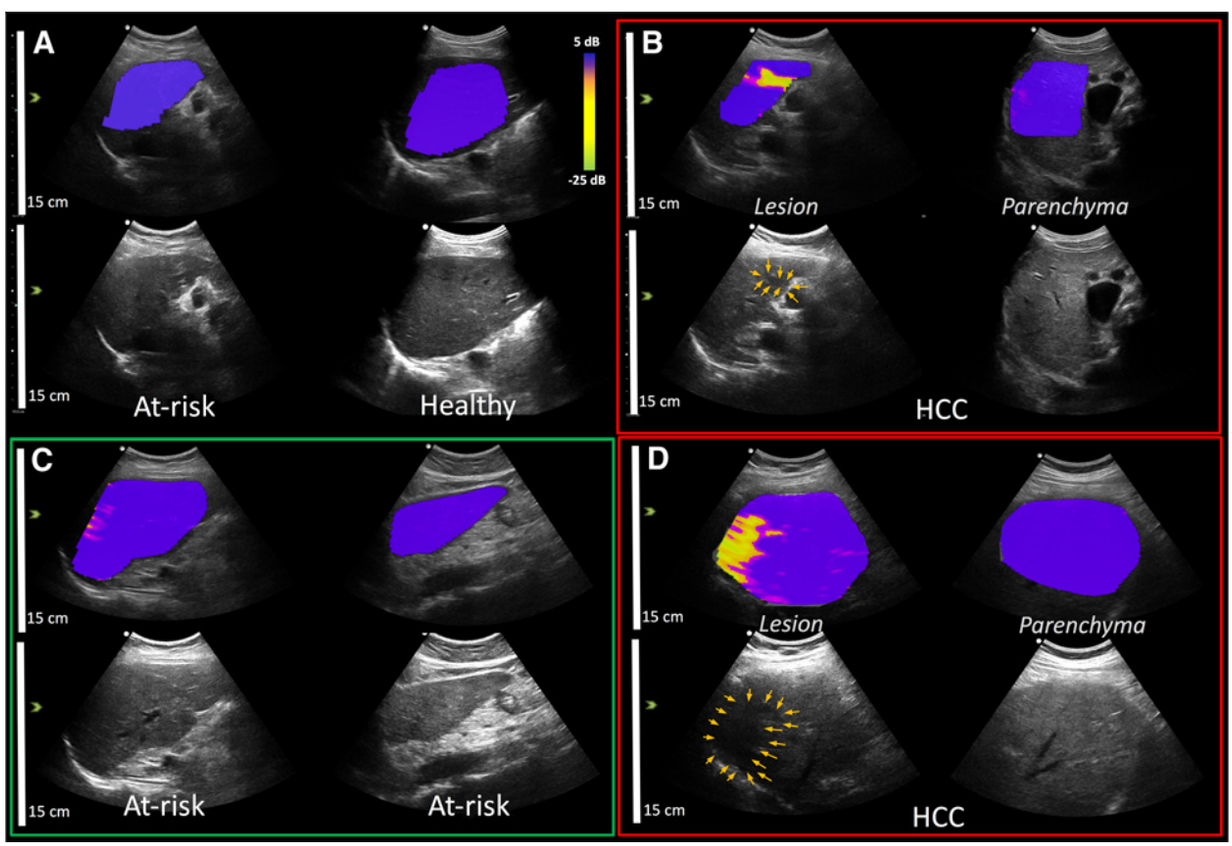

Figure 3.

Representative examples of parametric maps of the MBF parameter (threshold range of −25 dB to 5 dB) in five patients. Standard B-mode images (bottom rows) and B-mode images with overlaid parametric maps of the MBF QUS parameter (top rows) are displayed. The dynamic range of parametric maps is consistent in all images in the top row. Images are from (**A**) an at-risk patient (24-year-old female with chronic hepatitis (left) and in a healthy volunteer (right; 36-year-old male), (**B**) a 65-year-old woman with cryptogenic liver cirrhosis and confirmed HCC in segment V, (**C**) an at-risk 58-year-old female with chronic hepatitis, and (**D**) a 48-year-old male with a chronic hepatitis C and a confirmed HCC in segment VIII. Note homogenously blue-purple signal in non-HCC parenchyma in a patient with HCC (top and bottom third/fourth column), and in at-risk patient or healthy volunteer. Note that in the patients with HCC (top and bottom third column), MBF within the HCC lesion is substantially different and appears in yellow color on parametric map within the region around the lesion, suggesting tissue morphologic alterations in that area due to lesion growth; whereas on the B-mode image, the 2.2 × 1.8 cm (**B**) small, slightly hypoechoic, and not well-defined lesions are difficult to detect.

with random effect of subject. Differences in QUS values obtained in HCC compared with non-HCC parenchyma in patients with HCC as well as in non-HCC parenchyma between the three groups were tested by a mixed-effects multivariable-regression model with random effect of imaging plane nested within lobe and within subject. Prediction of presence of HCC versus non-HCC in the ROI in HCC patients was tested based on a threshold by a multivariable logistic regression model adjusted for clustering within a subject, and included sensitivity, specificity, and 95% confidence interval (CI). Agreement between fasting and nonfasting measurements was assessed by the Bland–Altman method and calculation of the concordance correlation (ICC; unadjusted for clustering within subjects); ICC of 0–0.20 indicated no agreement; 0.21–0.40, poor agreement; 0.41–0.60, moderate agreement; 0.61–0.80, good agreement; and greater than 0.80, excellent agreement. All statistical analyses were performed by using Stata 15 (StataCorp LP) and R version 3.3.1 (r-project.org). Statistical significance was fulfilled at $P < 0.05$.

Results

We obtained QUS parameters from the NPS at different spatial locations within user-selected ROIs. Figure 2 exhibits representative NPS from the orange (normal tissue) and yellow (lesion) ROI in a 65-year-old woman with cryptogenic liver cirrhosis and confirmed HCC in segment V.

Representative processed liver parametric maps of the MBF QUS parameter (obtained from the NPS) along with associated standard B-mode images are displayed in Fig. 3 and Supplementary Fig. S2. Images are from an at-risk patient (24-year-old female with chronic hepatitis B) and in a healthy volunteer (36-year-old male; Fig. 3A), a 65-year-old woman with cryptogenic liver cirrhosis and confirmed HCC in segment V, (Fig. 3B), an at-risk 58-year-old female with chronic hepatitis C (Fig. 3C), and a 73-year-old male with a chronic hepatitis C and a confirmed HCC in segment VIII (Fig. 3D). The parametric map displays a homogenously blue-purple signal in non-HCC parenchyma in patients from all three groups, whereas in the patient with HCC MBF within the HCC lesion is substantially different and appears in yellow color on parametric map; whereas on the B-mode image, the slightly hypoechoic and not well-defined lesion is difficult to detect.

Quantitative analysis, which is the primary goal of our study, is summarized in box-and-whiskers graphs in Fig. 4, which show the mean MBF, SI, and SS values obtained in normal liver parenchyma in the three patient groups and in HCC lesions. Table 2 shows the summary of mean values for the latter three QUS parameters. Note that all three parameters were significantly different in HCC versus non-HCC parenchyma but not within the three groups of non-HCC liver parenchyma.

More specifically, when comparing HCC lesion tissue with surrounding parenchyma, we observed that QUS parameters were significantly lower in HCC compared with adjacent non-HCC liver parenchyma measured in the same as well as the contralateral liver lobe (MBF, $P < 0.001$; SI, $P < 0.001$; and SS, $P < 0.001$). Similarly, MBF ($P < 0.001$), SI ($P < 0.001$), and SS ($P < 0.001$) values were significantly lower in HCC compared with non-HCC parenchyma in at-risk and healthy volunteers, independent of the liver lobe ($P < 0.001$). In addition, the prediction of the presence of HCC in patients with HCC was excellent for MBF using a cutoff of <0 dB [sensitivity, 94% (95% CI, 91%–97%); specificity, 100% (95% CI, 99%–100%)] and for SI using a cutoff of < 12 dB [sensitivity, 97% (95% CI, 94%–99%); specificity, 100% (95% CI, 99%–100%)]; and good for SS using a cutoff of > −2 dB/MHz [sensitivity, 71% (95% CI, 64%–76%); specificity, 86% (95% CI, 83%–89%)].

We next assessed whether different measures related to the patient or imaging influenced QUS parameters. Adjusted for age, gender, body mass index, focal depth, frame number frequency, plane, and presence of liver cirrhosis, the focal depth (9 vs. 3 cm) was the only parameter that had a statistically significant effect on MBF (weight, 0.27; 95% CI, 0.05–0.48; $P = 0.014$) and SS (weight, 0.1; 95% CI, 0.0–0.2; $P = 0.046$), but not on SI ($P = 0.934$). No other variables influenced QUS parameters in differentiating HCC and non-HCC parenchyma ($P > 0.05$). It is important to note that even liver cirrhosis had no effect on QUS parameters ($P > 0.827$). In addition, QUS parameter measures obtained in non-HCC parenchyma obtained from both liver lobes were not significantly different for MBF ($P = 0.89$), SI ($P = 0.14$), and SS ($P = 0.61$).

We also assessed whether fasting had an effect on QUS parameters. In an intraindividual comparison of QUS parameters obtained from the same liver when patient was in a fasting state versus nonfasting state, we observed an excellent agreement for MBF (ICC, 0.9; 95% CI, 0.88–0.92) and good agreement for SI

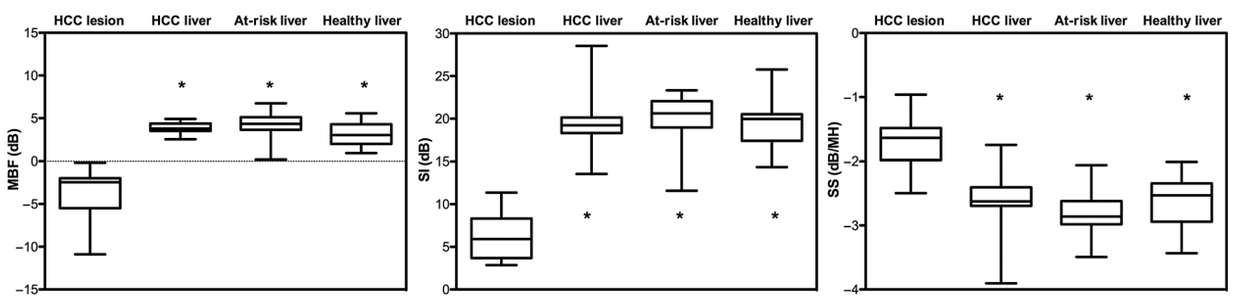

Figure 4.

Box-and-whiskers graphs summarize mean MBF (left), SI (middle), and SS (right) values obtained in normal liver parenchyma in the three patient groups and in HCC lesions. Note that all three parameters were significantly different in HCC versus non-HCC parenchyma but not within the three groups of non-HCC liver parenchyma. The ends of the box are the upper and lower quartiles; the vertical line inside the box represents the median; and the whiskers extend to the highest and lowest values. *, $P < 0.001$.

(ICC, 0.79; 95% CI, 0.76–0.82) and SS (ICC, 0.68; 95% CI, 0.63–0.72). This suggests that QUS parameters from liver parenchyma are not affected by fasting state.

Finally, we compared QUS parameter measures in non-HCC liver parenchyma among all groups. Adjusting for age, gender, focal depth, frame number, frequency, imaging plane, and presence of liver cirrhosis, there were no significant differences among the three groups in non-HCC liver parenchyma for MBF ($P = 0.12$), SI ($P = 0.33$), and SS ($P = 0.57$). Again, we noted that focal depth influenced MBF, SI, and SS values ($P < 0.001$). Unlike in HCC lesions, the presence of liver cirrhosis ($P = 0.011$) and measurements in the different liver lobes (right vs. left; $P < 0.001$) had a significant effect on MBF values only.

Discussion

Our results suggest clinical feasibility of QUS in the liver of healthy volunteers, at-risk, and patients with HCC for differentiation between different tissues. The parameters MBF, SI, and SS were substantially different in HCC versus non-HCC parenchyma in both intraindividual and interindividual comparisons among the three study groups. Furthermore, preliminary pilot subanalysis indicates that QUS parameters, especially MBF, are independent of fasting status in healthy volunteers in non-HCC parenchyma as well as independent of presence of liver cirrhosis in at-risk and patients with HCC for differentiation of HCC versus non-HCC tissues.

The use of QUS in tissue characterization, and more specifically as a tool for radiology diagnostics in cancer management, has regained substantial attention in recent years (12, 24–26). Quantitative parameters extracted from QUS are related to the source of backscatter in tissue, which are representative of underlying tissue structure and morphology properties (12). This allows inferring quantitative tissue characteristic information from the RF ultrasound signal beyond conventionally qualitative B-mode images. QUS parameters have been demonstrated to be sensitive to subtle microstructural characteristics and alterations occurring in tissue due to biological responses and tissue morphology resulting from disease or treatment. These have been previously demonstrated in preclinical studies (14, 27, 28–30) and in a clinical setting including patients with prostate cancer [disease detection (31), and extent of the disease (17)], as well as colorectal, gastric, and breast cancer patients to detect lymph node metastases (12, 32). Furthermore, QUS can be used in clinic to evaluate cancer treatment response and help clinicians adapt cancer therapies and exchange ineffective treatment therapies at an early stage (12, 25, 26, 33).

QUS of the liver was first used in 1987 (34) to quantify the liver echogenicity in patients with diffuse liver disease and healthy volunteers. In following preclinical studies, QUS could detect and grade fatty liver disease (35, 36). In a recent study (37), QUS was accurate in diagnosing and quantifying hepatic steatosis in humans with nonalcoholic fatty liver disease.

In this work, QUS parameters were computed from the power spectrum of raw RF-based B-mode images, and include the SS, the MBF, and the 0-MHz SI, which are respectively proportional to scatterer size, density, or both (12, 24). Several studies have now correlated these parameters to actual tissue structural properties in histopathology (i.e., size and density of cells/nuclei), and later confirmed as the source of scattering (12, 17). To the best of our knowledge, this study shows for the first time a substantial difference in QUS parameters in HCC versus non-HCC liver parenchyma in at-risk patients and healthy volunteers; and most importantly, this was independent of the presence of a cirrhotic liver background. The influence of focal depth on QUS parameters is expected, because of the depth-dependent alteration in attenuation. Small observed effects of age on QUS measurements in non-HCC liver tissues were interpreted as biased due to variations in the mean age across the three groups of patients. The influence of fasting on QUS parameters was evaluated for the first time by repeatedly scanning healthy fasting volunteers before and after food intake. Results suggested good (SI and SS) to excellent (MBF) agreement in QUS parameters among the two pre- and postprandial exams. This further suggests that QUS parameters are well reproducible when the same patient is imaged at two separate events. We observed that in QUS parametric maps, regions slightly larger than the identified lesion were contrasted; this is likely due to tissue morphologic alterations or abnormalities beyond the growing lesion border. Taken together, we showed that QUS could be used to detect the presence of HCC in patients with HCC with good sensitivity and specificity.

We acknowledge the following limitations to our study. First, due to the proof-of-principle nature of our study, only a small patient population size could be assessed with a wide range of tumor sizes. Further confirmatory studies are needed with a larger sample size. Second, we have not analyzed the feature validation of other liver lesions like regenerative or dysplastic nodules, intrahepatic cholangiocarcinoma, or metastasis; this has yet to be performed in future studies. Third, the sensitivity analysis was biased by a nonblinded radiologist regarding presence and location of HCC lesions. However, strong differences in quantitative parameters obtained in HCC and liver parenchyma are promising with additional prospective trials warranted to assess true prospective sensitivity and specificity of QUS in detecting HCC. Finally, other quantitative ultrasound parameters that are closely related to the effective scatterer size and scatter concentration can be computed when attenuation measurements are available and may add additional diagnostic information. These were not examined in this work and will be the topic of future studies.

In conclusion, our results suggest that QUS of the liver using the MBF, SI, and SS parameters allows differentiation between HCC and non-HCC liver parenchyma, at-risk liver, and normal liver parenchyma. This is independent of the status of the non-HCC liver parenchyma (cirrhotic vs. noncirrhotic; at-risk or normal) and the fasting state of the patient in healthy volunteers. QUS could be included in routine ultrasound screening protocols of the liver for HCC surveillance (where sweeps are used to survey most of the liver) in at-risk patients without extending the acquisition time, because QUS methods rely on the acquisition of conventional B-mode ultrasound images and accompanying RF data, making QUS a low-cost feature addition to commercial scanners, because virtually all systems currently perform strain elastography and therefore have the digital RF data available. In particular, in patients with cirrhotic liver parenchyma where standard B-mode ultrasound screening may be limited, QUS may add quantitative information and clinical value. Future developments of advanced algorithms and other QUS parameters could be used to automatically analyze the acquired data sets and guide the radiologist for better detection and further work-up of HCC.

Disclosure of Potential Conflicts of Interest

A. El Kaffas is an employee/paid consultant for Oncoustics, Inc. No potential conflicts of interest were disclosed by the other authors.

Authors' Contributions

Conception and design: I. Durot, A. El Kaffas
Development of methodology: I. Durot, N. Kothary, A. El Kaffas
Acquisition of data (provided animals, acquired and managed patients, provided facilities, etc.): I. Durot, R.M.S. Sigrist, N. Kothary, A. El Kaffas
Analysis and interpretation of data (e.g., statistical analysis, biostatistics, computational analysis): I. Durot, J. Rosenberg
Writing, review, and/or revision of the manuscript: I. Durot, R.M.S. Sigrist, A. El Kaffas
Administrative, technical, or material support (i.e., reporting or organizing data, constructing databases): I. Durot, A. El Kaffas
Study supervision: I. Durot
Other (study cosupervision with Dr. Willmann): A. El Kaffas

Acknowledgments

I. Durot was supported by the Swiss Society of Radiology. Oncoustics provided support through a Grand Challenges Canada grant subaward. Authors not affiliated with Oncoustics had full control of data acquisition, analysis, results, and outcome/findings.

The costs of publication of this article were defrayed in part by the payment of page charges. This article must therefore be hereby marked *advertisement* in accordance with 18 U.S.C. Section 1734 solely to indicate this fact.

Received March 27, 2019; revised May 23, 2019; accepted August 20, 2019; published first August 23, 2019.

References

1. Fateen W, Ryder SD. Screening for hepatocellular carcinoma: patient selection and perspectives. J Hepatocell Carcinoma 2017;4:71–9.
2. Ferlay J, Soerjomataram I, Dikshit R, Eser S, Mathers C, Rebelo M, et al. Cancer incidence and mortality worldwide: sources, methods and major patterns in GLOBOCAN 2012. Int J Cancer 2015;136:E359–86.
3. Kapitanov T, Neumann UP, Schmeding M. Hepatocellular carcinoma in liver cirrhosis: surgical resection versus transarterial chemoembolization-a meta-analysis. Gastroenterol Res Pract 2015;2015:696120.
4. Pinter M, Trauner M, Peck-Radosavljevic M, Sieghart W. Cancer and liver cirrhosis: implications on prognosis and management. ESMO Open 2016; 1:e000042.
5. Lang K, Danchenko N, Gondek K, Shah S, Thompson D. The burden of illness associated with hepatocellular carcinoma in the United States. J Hepatol 2009;50:89–99.
6. Kew MC. Hepatocellular carcinoma in developing countries: prevention, diagnosis and treatment. World J Hepatol 2012;4:99–104.
7. Expert Panel on Gastrointestinal I, Horowitz JM, Kamel IR, Arif-Tiwari H, Asrani SK, Hindman NM, et al. ACR appropriateness criteria((R)) chronic liver disease. J Am Coll Radiol 2017;14:S391–S405.
8. El-Serag HB. Epidemiology of viral hepatitis and hepatocellular carcinoma. Gastroenterology 2012;142:1264–73e1.
9. Yu SJ. A concise review of updated guidelines regarding the management of hepatocellular carcinoma around the world: 2010–2016. Clin Mol Hepatol 2016;22:7–17.
10. Soresi M, Terranova A, Licata A, Serruto A, Montalto G, Brancatelli G, et al. Surveillance program for diagnosis of HCC in liver cirrhosis: role of ultrasound echo patterns. Biomed Res Int 2017;2017: 4932759.
11. Singal A, Volk ML, Waljee A, Salgia R, Higgins P, Rogers MA, et al. Meta-analysis: surveillance with ultrasound for early-stage hepatocellular carcinoma in patients with cirrhosis. Aliment Pharmacol Ther 2009;30:37–47.
12. Oelze ML, Mamou J. Review of quantitative ultrasound: envelope statistics and backscatter coefficient imaging and contributions to diagnostic ultrasound. IEEE Trans Ultrason Ferroelectr Freq Control 2016;63:336–51.
13. Lizzi FL, Greenebaum M, Feleppa EJ, Elbaum M, Coleman DJ. Theoretical framework for spectrum analysis in ultrasonic tissue characterization. J Acoust Soc Am 1983;73:1366–73.
14. Gangeh MJ, Hashim A, Giles A, Sannachi L, Czarnota GJ. Computer aided prognosis for cell death categorization and prediction in vivo using quantitative ultrasound and machine learning techniques. Med Phys 2016;43:6439.
15. Muleki-Seya P, Guillermin R, Guglielmi J, Chen J, Pourcher T, Konofagou E, et al. High-frequency quantitative ultrasound spectroscopy of excised canine livers and mouse tumors using the structure factor model. IEEE Trans Ultrason Ferroelectr Freq Control 2016;63:1335–50.
16. Yao LX, Zagzebski JA, Madsen EL. Backscatter coefficient measurements using a reference phantom to extract depth-dependent instrumentation factors. Ultrason Imaging 1990;12:58–70.
17. Sadeghi-Naini A, Sofroni E, Papanicolau N, Falou O, Sugar L, Morton G, et al. Quantitative ultrasound spectroscopic imaging for characterization of disease extent in prostate cancer patients. Transl Oncol 2015;8: 25–34.
18. King DL, Lizzi FL, Feleppa EJ, Wai PM, Yaremko MM, Rorke MC, et al. Focal and diffuse liver disease studied by quantitative microstructural sonography. Radiology 1985;155:457–62.
19. Poullos PD, Tseng JJ, Melcher ML, Concepcion W, Loening AM, Rosenberg J, et al. Structured reporting of multiphasic CT for hepatocellular carcinoma: effect on staging and suitability for transplant. AJR Am J Roentgenol 2018;210:766–74.
20. Kolios MC, Czarnota GJ. Potential use of ultrasound for the detection of cell changes in cancer treatment. Future Oncol 2009;5: 1527–32.
21. Dong F, Madsen EL, MacDonald MC, Zagzebski JA. Nonlinearity parameter for tissue-mimicking materials. Ultrasound Med Biol 1999;25:831–8.
22. Lizzi FL, Astor M, Liu T, Deng C, Coleman DJ, Silverman RH. Ultrasonic spectrum analysis for tissue assays and therapy evaluation. Int J Imag Syst Tech 1997;8:3–10.
23. Lizzi FL, Feleppa EJ, Alam SK, Deng CX. Ultrasonic spectrum analysis for tissue evaluation. Pattern Recogn Lett 2003;24:637–58.
24. Jonathan Mamou MLO. Quantitative ultrasound in soft tissues. In:Jonathan Mamou MLO, editor. Quantitative ultrasound in soft tissues. New York, NY: Springer; 2013. p.443–639.
25. Sadeghi-Naini A, Papanicolau N, Falou O, Zubovits J, Dent R, Verma S, et al. Quantitative ultrasound evaluation of tumor cell death response in locally advanced breast cancer patients receiving chemotherapy. Clin Cancer Res 2013;19:2163–74.
26. Sadeghi-Naini A, Sannachi L, Pritchard K, Trudeau M, Gandhi S, Wright FC, et al. Early prediction of therapy responses and outcomes in breast cancer patients using quantitative ultrasound spectral texture. Oncotarget 2014;5: 3497–511.
27. Czarnota GJ, Kolios MC, Abraham J, Portnoy M, Ottensmeyer FP, Hunt JW, et al. Ultrasound imaging of apoptosis: high-resolution non-invasive monitoring of programmed cell death in vitro, in situ and in vivo. Br J Cancer 1999;81:520–7.
28. Banihashemi B, Vlad R, Debeljevic B, Giles A, Kolios MC, Czarnota GJ. Ultrasound imaging of apoptosis in tumor response: novel preclinical monitoring of photodynamic therapy effects. Cancer Res 2008;68: 8590–6.
29. Lavarello RJ, Ridgway WR, Sarwate SS, Oelze ML. Characterization of thyroid cancer in mouse models using high-frequency quantitative ultrasound techniques. Ultrasound Med Biol 2013;39: 2333–41.
30. Tran WT, Sannachi L, Papanicolau N, Tadayyon H, Al Mahrouki A, El Kaffas A, et al. Quantitative ultrasound imaging of therapy response in bladder cancer in vivo. Oncoscience 2016;3:122–33.
31. Feleppa EJ, Mamou J, Porter CR, Machi J. Quantitative ultrasound in cancer imaging. Semin Oncol 2011;38:136–50.

32. Saegusa-Beecroft E, Machi J, Mamou J, Hata M, Coron A, Yanagihara ET, et al. Three-dimensional quantitative ultrasound for detecting lymph node metastases. J Surg Res 2013;183:258–69.
33. Tadayyon H, Sannachi L, Gangeh MJ, Kim C, Ghandi S, Trudeau M, et al. A priori prediction of neoadjuvant chemotherapy response and survival in breast cancer patients using quantitative ultrasound. Sci Rep 2017;7: 45733.
34. Garra BS, Insana MF, Shawker TH, Russell MA. Quantitative estimation of liver attenuation and echogenicity: normal state versus diffuse liver disease. Radiology 1987;162(1 Pt 1):61–7.
35. Ghoshal G, Lavarello RJ, Kemmerer JP, Miller RJ, Oelze ML. Ex vivo study of quantitative ultrasound parameters in fatty rabbit livers. Ultrasound Med Biol 2012;38:2238–48.
36. Weijers G, Starke A, Thijssen JM, Haudum A, Wohlsein P, Rehage J, et al. Transcutaneous vs. intraoperative quantitative ultrasound for staging bovine hepatic steatosis. Ultrasound Med Biol 2012;38:1404–13.
37. Lin SC, Heba E, Wolfson T, Ang B, Gamst A, Han A, et al. Noninvasive diagnosis of nonalcoholic fatty liver disease and quantification of liver fat using a new quantitative ultrasound technique. Clin Gastroenterol Hepatol 2015;13:1337–45e6.